A conservative diffuse-interface method for the simulation of compressible two-phase flows with turbulence and acoustics

By S. S. Jain, A. Mani AND P. Moin

1. Motivation and objectives

Prediction of bubble dynamics in turbulent seawater is of practical importance for the engineering analysis of naval systems. In ships, the air bubbles entrained by boundary layers and stern waves form an elongated wake that lasts for several kilometers downstream (Trevorrow *et al.* 1994; Fu *et al.* 2007; Stanic *et al.* 2009). Though the bubbles are tiny, with diameters of order 1 mm or less, they exhibit strong acoustic responses and hence the bubbly wake can be detected acoustically, which reveals the presence and position of the ship (Figure 1). The predictive modeling of bubble distributions in wakes, along with their acoustic response, has remained elusive and mostly confined to Reynolds-averaged Navier-Stokes (RANS) analyses because of the multiscale nature of the problem and the computational challenges associated with scalability and performance (Carrica *et al.* 1999; Culver & Trujillo 2007). Hence, the focus of the current study is to develop a conservative numerical method that enables accurate treatment of the interaction of acoustics with gas-liquid interfaces (single and multiple bubbles) in compressible turbulent flow environments. This aids in investigating the current limitations and in developments of subgrid-scale models based on the Rayleigh-Plesset or Keller-Miksis equations used in RANS and large eddy simulations (LES).

Apart from bubble acoustics, applications of compressible two-phase flows also include supercritical flow regimes in high-pressure environments and liquid fuel injection systems. In compressible flows, thermodynamics plays an important role and adds one more level of difficulty to an already complex problem of two-phase flows, by imposing an additional requirement that the model should maintain thermodynamic consistency at the interface. Moreover, the numerical study of turbulent flows and acoustics requires stable, non-dissipative, and conservative numerical methods. To the best of our knowledge, the state-of-the-art techniques to simulate compressible two-phase flows lack many of these features. With this motivation, we have developed a diffuse-interface five-equation model for the simulation of two immiscible compressible fluids that (a) can be solved using non-dissipative numerical methods (low- and high-order central-difference schemes), (b) discretely conserves mass of each phase, total momentum, and total energy in the system, (c) maintains mechanical equilibrium and thermodynamic equilibrium across the interface, and (d) maintains a steady interface thickness throughout the simulation.

2. Literature review

Compressible two-phase flows have been extensively studied for the last two decades (Saurel & Pantano 2018). Different diffuse-interface models present in the literature can be broadly classified into four major types: (a) The five-equation model (Kapila *et al.*

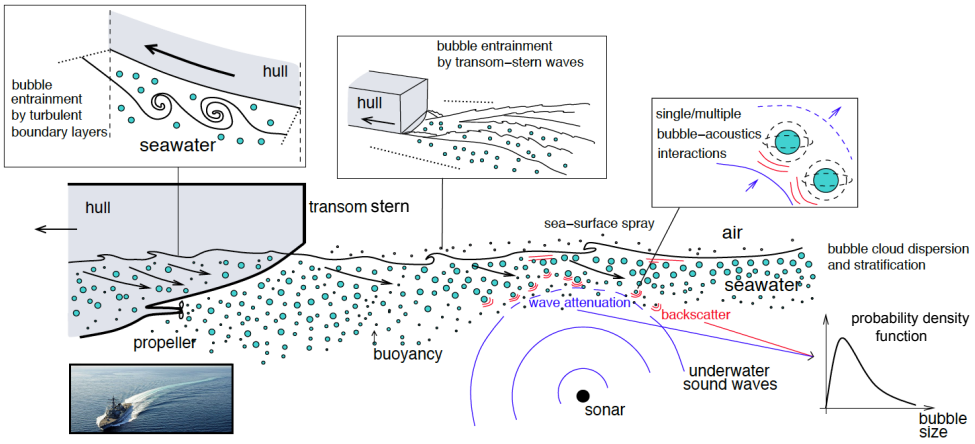

FIGURE 1. Schematics of the generation of bubbly wakes from the stern of a ship, including the associated interactions between bubbles and acoustic waves, the latter being generated from an underwater sonar.

2001) solves two mass balance equations—one for each of the phases —a momentum equation, a total energy equation, and a volume fraction advection equation. This is the model that is most suitable for the simulation of two-phase non-reacting flows with immiscible fluids. This model is discussed further in Section 3. (b) The six-equation model is similar to the five-equation model but solves two energy equations, one for each of the phases. (c) The seven-equation model (Baer & Nunziato 1986) solves two momentum equations and two energy equations and has two separate velocity fields for each of the phases. This is the most general of all the models since it includes non-equilibrium effects such as phase change and mass transfer. (d) The four-equation model (Abgrall 1996) has no separate mass balance equations for each of the phases; instead, it solves a continuity equation, hence conserving only the total mass and not the individual mass of each phase. The volume fraction advection equation has also been replaced by a transport equation for the polytropic coefficient in this model. Further, many improvements have been proposed for all these models in the literature. A detailed review is beyond the scope of this article and will be included in future work.

Attempts to simulate compressible two-phase flows have also been made using sharp-interface methods; see Jemison *et al.* (2014) for the moment-of-fluid approach, Herrmann (2016) for a geometric volume-of-fluid approach, Huber *et al.* (2015) and Fu *et al.* (2017) for a level-set method, and He *et al.* (2017) for an algebraic volume-of-fluid approach. Although, sharp-interface methods are more accurate than diffuse-interface methods, they are also more expensive. Moreover, the expensive function evaluation of the sharp-interface methods is localized at the interface, which results in load-balancing and parallel scalability issues. When it comes to compressible flows, diffuse-interface methods have an obvious advantage over sharp-interface methods. The volume of each phase is inherently not conserved in compressible flows; hence, the expensive interface reconstruction and the geometric advection step in sharp-interface methods to achieve discrete volume conservation are less useful. Moreover, one cannot achieve mass conservation of each phase using a sharp-interface method —with the exception of the moment-of-fluid method (Jemison

et al. 2014) —whereas, depending on the choice of the model, a mass balance equation in each phase can be solved in a diffuse-interface method to discretely conserve the mass of each phase. For these reasons, in the current study, we choose to use a diffuse-interface method over a sharp-interface method. For a more detailed comparison between sharp-interface and diffuse-interface methods, see Mirjalili *et al.* (2017).

In summary, a five-equation model appears to be the preferred choice of diffuse-interface model for the simulation of compressible two-phase flows with immiscible fluids. Some of the limitations in the current state-of-the-art methods are as follows: (a) The study of acoustics and turbulent flows requires non-dissipative methods, but to the best of our knowledge, there is no previous implementation of compressible two-phase flows that is non-dissipative (central-difference schemes). (b) All the sharpening terms (interface regularization) used along with the five-equation model are in non-conservative form (Shukla *et al.* 2010; Tiwari *et al.* 2013), and the conservative form of the sharpening terms is currently considered to be unstable (Shukla *et al.* 2010). (c) None of the previous studies explore compressible two-phase flows in a turbulent environment.

3. Conservation equations

We start with the well-known inviscid five-equation model of Allaire *et al.* (2002). This form of the model has a volume fraction advection equation [Eq. (3.1)], a mass balance equation for each of the phases l [Eq. (3.2)], a momentum equation [Eq. (3.3)], and a total energy equation [Eq. (3.4)].

$$\frac{\partial \phi_1}{\partial t} + \vec{u} \cdot \vec{\nabla} \phi_1 = 0, \tag{3.1}$$

$$\frac{\partial \rho_l \phi_l}{\partial t} + \vec{\nabla} \cdot (\rho_l \vec{u} \phi_l) = 0, \qquad l = 1, 2, \tag{3.2}$$

$$\frac{\partial \rho \vec{u}}{\partial t} + \vec{\nabla} \cdot (\rho \vec{u} \otimes \vec{u} + p \mathbb{1}) = 0, \tag{3.3}$$

and

$$\frac{\partial \rho (e + k)}{\partial t} + \vec{\nabla} \cdot (\rho H \vec{u}) = 0, \tag{3.4}$$

where ϕ_l is the volume fraction of phase l that satisfies the condition $\sum_{l=1}^{2} \phi_l = 1$, ρ_l is the density of phase l, ρ is the total density defined as $\rho = \sum_{l=1}^{2} \rho_l \phi_l$, $\vec{u}$ is the velocity, p is the pressure, e is the specific mixture internal energy, which can be related to the specific internal energy of phase l e_l as $e = \sum_{l=1}^{2} \rho_l e_l$, $k = \frac{1}{2} u_i u_i$ is the specific kinetic energy, and $H = e + k + p/\rho$ is the specific total enthalpy of the mixture.

Allaire *et al.* (2002) showed that when this system is solved along with an isobaric closure law at the interface, one can achieve mechanical and thermodynamic equilibrium (Postulate 3.1) at the interface that results in stable numerical solutions and eliminates spurious oscillations at the interface.

POSTULATE 3.1. *If $u_i^k = u_0$ and $p_i^k = p_0$ across the interface, any model or a numerical scheme that satisfies $u_i^{k+1} = u_0$ and $p_i^{k+1} = p_0$, $\forall i$, is said to satisfy the interface equilibrium condition (IEC), where k is the timestep index and i is the grid index (see Abgrall 1996).*

It is generally known that the interface thickness increases with simulation time in

a classical diffuse-interface method, reducing the accuracy of the solution for long-time integrations. Hence, Shukla *et al.* (2010) and Tiwari *et al.* (2013) proposed interface-sharpening terms to counter this thickening of the interface. However, the sharpening terms are in non-conservative form, and they argued that the conservative form of the interface-sharpening (regularization) terms results in tangential fluxes, which leads to unphysical interface deformations.

In the current work, we propose a new set of sharpening terms that are in conservative form and show that the numerical solution is stable for long-time integrations. We propose a model of the form given in Eqs. (3.5)–(3.8) along with the viscous terms, where the highlighted terms are the newly introduced sharpening (regularization) terms. Equation (3.5) represents the modified volume fraction advection equation, Eq. (3.6) represents the modified mass balance equation for phase l, Eq. (3.7) represents the modified momentum equation, and Eq. (3.8) represents the modified total energy equation. If a general equation of state (EOS) for phase l is written as $p_l = \alpha_l \rho_l e_l + \beta_l$, where α_l and β_l are constants, then by invoking the isobaric closure law for pressure in the mixture region ($p = p_1 = p_2$), the generalized mixture EOS can be written as in Eq. (3.9).

$$\frac{\partial \phi_1}{\partial t} + \vec{\nabla} \cdot (\vec{u}\phi_1) = \phi_1(\vec{\nabla} \cdot \vec{u}) + \vec{\nabla} \cdot \vec{a_1}, \tag{3.5}$$

$$\frac{\partial m_l}{\partial t} + \vec{\nabla} \cdot (\vec{u} m_l) = \vec{\nabla} \cdot R_l, \qquad l = 1, 2, \tag{3.6}$$

$$\frac{\partial \rho \vec{u}}{\partial t} + \vec{\nabla} \cdot (\rho \vec{u} \otimes \vec{u} + p\mathbb{1}) = \vec{\nabla} \cdot \underline{\underline{\tau}} + \vec{\nabla} \cdot (\vec{f} \otimes \vec{u}), \tag{3.7}$$

$$\frac{\partial E}{\partial t} + \vec{\nabla} \cdot (\vec{u}E) + \vec{\nabla} \cdot (p\vec{u}) = \vec{\nabla} \cdot (\vec{f}k) + \vec{\nabla} \cdot (\underline{\underline{\tau}} \cdot \vec{u}) + \sum_{l=1}^{2} \vec{\nabla} \cdot (\rho_l h_l \vec{a}_l), \tag{3.8}$$

and

$$p = \frac{\rho e + \left(\frac{\phi \beta_1}{\alpha_1} + \frac{(1-\phi)\beta_2}{\alpha_2} \right)}{\left(\frac{\phi}{\alpha_1} + \frac{1-\phi}{\alpha_2} \right)}. \tag{3.9}$$

In Eqs. (3.5)–(3.8), $\vec{a}_1 = \Gamma\{\epsilon \vec{\nabla}\phi_1 - \phi_1(1-\phi_1)\vec{n}\}$ is the flux of the interface regularization term for phase 1, and it satisfies the condition $\vec{a}_1 = -\vec{a}_2$, $\vec{n} = \vec{\nabla}\phi/|\vec{\nabla}\phi|$ is the outward normal of the interface, and Γ and ϵ are the interface parameters (see Section 4 for a discussion of the choice of these parameters). $R_l = \rho_{0l}\vec{a}_l$ is the flux of the regularization term in the mass equation for phase l, where ρ_{0l} is the characteristic density representing phase l (see Section 5), $\vec{f} = \sum_{l=1}^{2} R_l$ is the net mass regularization flux, $m_l = \rho_l \phi_l$ is the mass per unit total volume for phase l, and $\rho = \sum_{l=1}^{2} m_l$ is the total density of the mixture. In Eq. (3.6), m_l is written instead of $\rho_l \phi_l$ only to show that m_l is the variable being solved and not ρ_l (see Section 5). The Cauchy stress tensor is written as $\underline{\underline{\tau}} = 2\mu\mathbb{D} - 2\mu(\vec{\nabla} \cdot \vec{u})\mathbb{1}/3$, where μ is the dynamic viscosity of the mixture evaluated using the one-fluid mixture rule as $\mu = \sum_{l=1}^{2} \phi_l \mu_l$, $\mathbb{D} = \{(\vec{\nabla}\vec{u}) + (\vec{\nabla}\vec{u})^T\}/2$ is the strain-rate tensor, and $E = \rho(e + k)$ is the total energy per unit volume. If each of the phases is assumed to follow a stiffened gas EOS, then the constants in the EOS can be written as $\alpha = \gamma - 1$ and $\beta = -\gamma\pi$, where γ is the polytropic coefficient and π is the reference pressure. Values of γ and π are experimentally determined, and the values used in this

work are listed in Table 1. Then, the speed of sound c_l for phase l can be written as

$$c_l = \sqrt{\gamma_l \Big(\frac{p + \pi_l}{\rho_l} \Big)}. \tag{3.10}$$

In Eq. (3.8), $h_l = e_l + p/\rho_l$ represents the specific enthalpy of the phase l and can be expressed in terms of ρ_l and p using the EOS as

$$h_l = \frac{(p + \pi_l)\gamma_l}{\rho_l(\gamma_l - 1)}. \tag{3.11}$$

All the newly added terms are in conservative form, and hence the mass of each phase, momentum, and total energy are discretely conserved in the simulation irrespective of the choice of the numerical scheme. Moreover, we choose to use a second-order central-difference scheme for all the discretizations in this study since low-order central-difference schemes are known to have some advantages for the simulation of turbulent flows (Moin & Verzicco 2016) due to their (a) non-dissipative nature, (b) low aliasing error, (c) easy boundary treatment, (d) low cost, and (e) improved stability. The non-dissipative nature of these schemes is also crucial for the resolved simulation of acoustics.

Further, a systematic derivation of the newly introduced regularization terms, along with the proof of boundedness of ϕ_l and the proof of the IEC, is described in Sections 4–8.

4. Volume fraction advection equation: Proof of boundedness of ϕ

If we denote the volume fraction of phase 1 ϕ_1 as ϕ, then the the volume fraction advection equation in Eq. (3.5) can be written as

$$\frac{\partial \phi}{\partial t} + \vec{\nabla} \cdot (\vec{u}\phi) = \phi(\vec{\nabla} \cdot \vec{u}) + \vec{\nabla} \cdot \Big[\Gamma \Big\{ \epsilon \vec{\nabla}\phi - \phi(1 - \phi)\vec{n} \Big\} \Big]. \tag{4.1}$$

This equation is obtained by combining Eq. (3.1) and the reinitialization step of the conservative level-set method by Olsson & Kreiss (2005) and Olsson *et al.* (2007), and is also an extension of the incompressible version of the conservative diffuse-interface method introduced by Mirjalili *et al.* (2018). One can show that Eq. (4.1) also governs the advection of the volume fraction for phase 2; i.e., $\phi_2 = 1 - \phi$ also satisfies Eq. (4.1). Hence, both phases 1 and 2 are consistently advected.

Since we choose to use a central-difference scheme to discretize all the system of equations in our model because of the well-known desirable properties, as already described in Section 3, this choice of the scheme could potentially create overshoots and undershoots in the ϕ field due to the dispersion errors. Hence, one needs to pick the values of the free parameters Γ and ϵ such that ϕ is maintained between 0 and 1.

Mirjalili *et al.* (2018) showed that there exists a crossover line in the ϵ-Γ parameter space above which the boundedness of ϕ is guaranteed for an incompressible flow. We extend this analysis to show that the same criterion (Figure 2) is sufficient to maintain the boundedness of the ϕ field in a compressible flow setting, provided that the timestep restriction given in Eq. (4.3) for a one-dimensional setting and Eq. (4.9) for a three-dimensional setting is satisfied (Theorem 4.1).

THEOREM 4.1. *On a uniform one-dimensional grid, if* $0 \leq \phi_i^k \leq 1$ *is satisfied for* $k = 0$*, then* $0 \leq \phi_i^k \leq 1$ *holds* $\forall k \in \mathbb{Z}^+$*, where* k *is the time-step index and* i *is the grid*

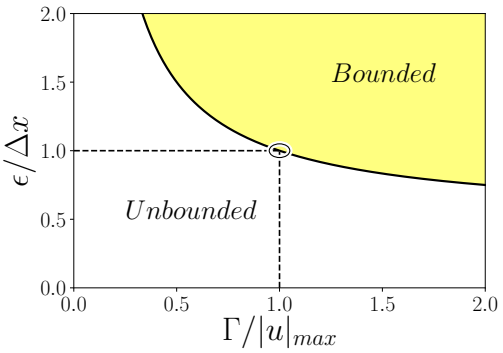

FIGURE 2. Region of boundedness as given by Eq. (4.2).

index, provided

$$\frac{\epsilon}{\Delta x} \geq \frac{1}{2}\left(\frac{|u|_{max}}{\Gamma} + 1\right) \tag{4.2}$$

and

$$\Delta t \leq \min_i \left\{ \left[\left(\frac{2\Gamma\epsilon}{\Delta x^2}\right) - \left(\frac{u_{i+1}^k - u_{i-1}^k}{2\Delta x}\right) \right]^{-1} \right\}, \tag{4.3}$$

are satisfied.

Proof. Consider the discretization of Eq. (4.1) on a one-dimensional uniform grid

$$\begin{aligned} \phi_i^{k+1} = \phi_i^k + \Delta t \Bigg[&- \Big(\frac{u_{i+1}^k \phi_{i+1}^k - u_{i-1}^k \phi_{i-1}^k}{2\Delta x}\Big) + \phi_i^k \Big(\frac{u_{i+1}^k - u_{i-1}^k}{2\Delta x}\Big) \Bigg] \\ + \Delta t \Big[\Gamma\epsilon \Big(\frac{\phi_{i+1}^k - 2\phi_i^k + \phi_{i-1}^k}{\Delta x^2}\Big) &- \Gamma \Big\{ \frac{(1-\phi_{i+1}^k) n_{i+1}^k \phi_{i+1}^k - (1-\phi_{i-1}^k) n_{i-1}^k \phi_{i-1}^k}{2\Delta x} \Big\} \Big], \end{aligned} \tag{4.4}$$

where k represents the time index and i the grid index. This can be rearranged as

$$\phi_i^{k+1} = \tilde{C}_{i-1}^k \phi_{i-1}^k + \tilde{C}_i^k \phi_i^k + \tilde{C}_{i+1}^k \phi_{i+1}^k, \tag{4.5}$$

where $\tilde{C}$'s are coefficients given by

$$\tilde{C}_{i-1}^k = \frac{\Delta t u_{i-1}^k}{2\Delta x} + \frac{\Delta t \Gamma \epsilon}{\Delta x^2} + \frac{\Delta t \Gamma}{2\Delta x}(1 - \phi_{i-1}^k) n_{i-1}^k, \tag{4.6}$$

$$\tilde{C}_{i+1}^k = -\frac{\Delta t u_{i+1}^k}{2\Delta x} + \frac{\Delta t \Gamma \epsilon}{\Delta x^2} - \frac{\Delta t \Gamma}{2\Delta x}(1 + \phi_{i+1}^k) n_{i+1}^k \tag{4.7}$$

and

$$\tilde{C}_i^k = 1 + \frac{\Delta t}{2\Delta x}(u_{i+1}^k - u_{i-1}^k) - \frac{2\Delta t \Gamma \epsilon}{\Delta x^2}. \tag{4.8}$$

LEMMA 4.1.1. *A scheme is said to be bounded if $\tilde{C}$'s are all positive (see Section 5.4.2 of Versteeg & Malalasekera 2007).*

For $k = 0$, it is given that $0 \leq \phi_i^k \leq 1$ holds, which implies that $(1 - \phi_{i-1}^k) n_{i-1}^k \geq -1$. Then $\tilde{C}_{i-1}^1 \geq \Delta t u_{i-1}^0/(2\Delta x) + \Delta t \Gamma \epsilon/\Delta x^2 - \Delta t \Gamma/(2\Delta x) \geq -\Delta t/2\Delta x(|u|_{max}^0 + \Gamma) +$

$\Delta t\Gamma\epsilon/\Delta x^2$. Now, invoking the condition in Eq. (4.2), we can show that $\tilde{C}^1_{i-1} \geq 0$ holds. Using similar arguments, we can show that $\tilde{C}^1_{i+1} \geq 0$ holds. Invoking the condition in Eq. (4.3), we can also show that $\tilde{C}^1_i \geq 0$ holds. Thus, Lemma 4.1.1 proves that $0 \leq \phi^1_i \leq 1$ is satisfied. Now, by repeating the same procedure above, we can show that $0 \leq \phi^{k+1}_i \leq 1$ is satisfied, provided that $0 \leq \phi^k_i \leq 1$ is satisfied. Hence, using mathematical induction, $0 \leq \phi^k_i \leq 1$ is satisfied $\forall k \in \mathbb{Z}^+$, which concludes the proof.

□

If ϕ is bounded, then $1-\phi$ is also bounded. Hence, the volume fractions of both phases 1 and 2 are bounded. Now, generalizing Theorem (4.1) for three dimensions, the timestep restriction required for the boundedness of ϕ can be written as

$$\Delta t \leq \min_i \left\{ \frac{1}{(\frac{6\Gamma\epsilon}{\Delta x^2}) - (\frac{\delta u_i}{\delta x_i})} \right\}, \tag{4.9}$$

where $\delta/\delta x$ is the discrete derivative operator. The first term $(6\Gamma\epsilon/\Delta x^2)$ represents the diffusive Courant–Friedrichs–Lewy (CFL) condition of the interface, with $\Gamma\epsilon$ representing the diffusivity of the interface regularization and the second term $(\delta u_i/\delta x_i)$ representing the time constraint associated with the local dilation of the flow. Hence, if the flow is expanding, the timestep constraint is less restrictive, and if the flow is compressing, then the timestep constraint is more restrictive. However, the timestep restriction due to the acoustic CFL condition in the flow is usually more restrictive than the condition in Eq. (4.9).

5. Mass balance equation

We employ a phenomenological approach to derive the mass balance equation for phase l [Eq. (3.6)]. Similar to Section 4, let $\phi = \phi_1$. Then, the mass per unit total volume of phase 1, is given by $m_1 = \rho_1\phi$. Now, starting with the mass balance equation of the form

$$\frac{\partial \rho_1\phi}{\partial t} + \vec{\nabla}\cdot(\rho_1\vec{u}\phi) = \vec{\nabla}\cdot\Big[\rho_1\Gamma\Big\{\epsilon\vec{\nabla}\phi - \phi(1-\phi)\vec{n}\Big\}\Big], \tag{5.1}$$

one can see that in the incompressible limit ($\rho_1 \to \rho_{01}$, $\vec{\nabla}\cdot\vec{u} = 0$), it is consistent with the volume fraction advection equation (Eq. (4.1)), where the characteristic density of phase 1 ρ_{01} is indeed the density of phase 1 in the incompressible limit. But one main disadvantage of this formulation is that it requires explicit computation of ρ_1. Typically, $m_1 = \rho_1\phi$ are solved together, and to obtain ρ_1, one should use $\rho_1 = m_1/\phi$, which results in inaccurate values of ρ_1 at the interface due to round-off errors (that stem from division by a small number). To overcome this, we use a form of the equation

$$\frac{\partial \rho_1\phi}{\partial t} + \vec{\nabla}\cdot(\rho_1\vec{u}\phi) = \vec{\nabla}\cdot\Big[\rho_{01}\Gamma\Big\{\epsilon\vec{\nabla}\phi - \phi(1-\phi)\vec{n}\Big\}\Big]. \tag{5.2}$$

This form of the equation also satisfies the same consistency condition in the limit of incompressibility and is similar to the one proposed in Eq. (5.1). Hence, we use this form of the mass equation since it does not require explicit computation of ρ_1. Now, writing Eq. (5.2) in terms of m, we get Eq. (3.6).

Further, summing up Eq. (3.6) for phases 1 and 2, we can derive the modified version of the continuity equation given by

$$\frac{\partial \rho}{\partial t} + \vec{\nabla}\cdot(\rho\vec{u}) = \vec{\nabla}\cdot\vec{f}, \tag{5.3}$$

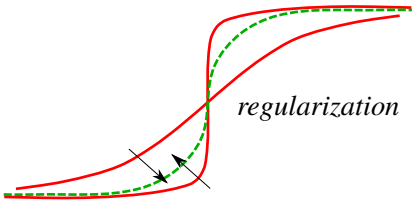

FIGURE 3. Schematic of effect of regularization terms on all quantities. Solid lines represent quantities before regularization and the dashed line represent the quantity after regularization.

where $\vec{f} = \sum_{l=1}^{2} R_l = \sum_{l=1}^{2} \rho_{0l}\vec{a}_l$ is the net mass regularization flux. The mass regularization flux for phase l, $R_l = \rho_{0l}\vec{a}_l$ in Eq. (3.7), can be intuitively thought to be a weighted version of the interface regularization flux $\vec{a}_l$ for phase l, where the weight is the characteristic density of the phase ρ_{0l}. This scaling of the flux is employed such that the timescales of regularization of the ϕ and ρ_l fields are similar.

The regularization terms are crucial in maintaining consistency between the mass and volume fraction fields. Figure 3 shows the effect of regularization terms on all the quantities being solved. Hence, if the volume fraction field is modified, reorganization of the mass is required to maintain consistency between the ρ and ϕ fields, which is essentially achieved with the use of the regularization terms.

6. Momentum equation

Since the momentum of each of the phases is not individually conserved due to exchange of momentum at the interface, it is most efficient to write a single momentum equation for both phases. One can start with the momentum equation of the form

$$\frac{\partial \rho\vec{u}}{\partial t} + \vec{\nabla}\cdot[(\rho\vec{u})\otimes\vec{u} + p\mathbb{1}] = 0, \tag{6.1}$$

in the inviscid limit. Taking the dot product of this equation with $\vec{u}$, and utilizing the modified continuity equation (Eq. (5.3)), results in the kinetic energy transport equation of the form

$$\frac{\partial \rho k}{\partial t} + \vec{\nabla}\cdot(\rho\vec{u}k) + k(\vec{\nabla}\cdot\vec{f}) + \vec{\nabla}\cdot(\vec{u}p) - p(\vec{\nabla}\cdot\vec{u}) = 0, \tag{6.2}$$

where, the non-conservative term $k(\vec{\nabla}\cdot\vec{f})$ represents the spurious contribution to the kinetic energy, which stems from the regularization of the interface. Having a spurious non-conservative term in the kinetic energy equation, even in the continuous form, is a sign that the solutions of this model could potentially be spurious. This allusion is correct since the form of the momentum equation in Eq. (6.1) does not satisfy the IEC.

Now, let's consider the modified version of momentum equation (Eq. (3.7)) in the inviscid limit

$$\frac{\partial \rho\vec{u}}{\partial t} + \vec{\nabla}\cdot[(\rho\vec{u} - \vec{f})\otimes\vec{u} + p\mathbb{1}] = 0. \tag{6.3}$$

Taking the dot product of this equation with $\vec{u}$ and utilizing the modified continuity equation (Eq. (5.3)), results in the kinetic energy transport equation of the form

$$\frac{\partial \rho k}{\partial t} + \vec{\nabla}\cdot[(\rho\vec{u} - \vec{f})k] + \vec{\nabla}\cdot(\vec{u}p) - p(\vec{\nabla}\cdot\vec{u}) = 0, \tag{6.4}$$

where there are no non-conservative terms that spuriously contribute to the kinetic energy. Additionally, the form of momentum equation in Eq. (3.7) also satisfies IEC (see Section 8), thus reinforcing the fact that the solution is not spuriously affected by regularization of the interface. This consistency correction to the momentum is crucial for compressible flows, without which the spurious momentum (or velocity) contribution to kinetic energy naturally leads to blow-up of the solver for any pair of fluids. However, this consistency requirement is not as severe for incompressible flows. This method has been shown to be stable for low-density ratio flows at low Re without this correction (Mirjalili *et al.* 2018). This could be due to the enforcement of the divergence-free condition for the velocity, which stabilizes the solver. However, for high-density ratio flows and at high Re, the consistency correction is also required for incompressible flows to stabilize the solver (Mirjalili *et al.* 2019). The discrete analogue of all the mathematical operations performed in this section will be presented in future work.

7. Energy equation: entropy conservation form

Entropy is not conserved in a diffuse-interface method even in the inviscid limit due to the regularization of the interface (irreversible process), which leads to the reorganization of mass, momentum, and potentially also energy, as illustrated in Figure 3. Entropy should only be conserved if the interface is already perfectly regular and the effects of all the regularization terms are identically zero. Thus, we seek to achieve approximate entropy conservation instead of exact conservation and derive the conservative form of the regularization terms in the energy equation with the constraint that it should satisfy he IEC. We first look at the case of exact entropy conservation and show that it doesn't satisfy the IEC, and then look at the case where the IEC is satisfied and then state that entropy is not conserved.

LEMMA 7.1. *Let s_l be the physical entropy and T_l be the temperature of phase l. Then the form of the internal energy equation that satisfies (entropy conservation)*

$$\sum_{l=1}^{2}\left[\rho_l\phi_l T_l\frac{Ds_l}{Dt}\right]=0 \tag{7.1}$$

in the inviscid limit is

$$\frac{\partial\rho e}{\partial t}+\vec{\nabla}\cdot(\rho\vec{u}e)+\vec{\nabla}\cdot(p\vec{u})-\vec{u}\cdot\vec{\nabla}p=\sum_{l=1}^{2}\left\{h_l\vec{\nabla}\cdot(\rho_l\vec{a}_l)\right\}. \tag{7.2}$$

Proof. Let the internal energy equation be of the form

$$\frac{D\rho e}{Dt}+\rho h(\vec{\nabla}\cdot\vec{u})+X=0, \tag{7.3}$$

where X is the unknown term to be determined. Expressing the internal energy in terms of phase quantities

$$\frac{D\rho e}{Dt}=\sum_{l=1}^{2}\frac{D(\phi_l\rho_l e_l)}{Dt}=\sum_{l=1}^{2}\left[\phi_l\frac{D(\rho_l e_l)}{Dt}+\rho_l e_l\frac{D\phi_l}{Dt}\right], \tag{7.4}$$

we then use Gibb's relation to get

$$\mathrm{d}(\rho_l e_l)=\rho_l\mathrm{d}e_l+e_l\mathrm{d}\rho_l=\rho_l T_l\mathrm{d}s_l+h_l\mathrm{d}\rho_l. \tag{7.5}$$

Using this in Eq. (7.3) results in

$$\sum_{l=1}^{2}\Big[\rho_l\phi_l T_l\frac{Ds_l}{Dt}+\phi_l h_l\frac{D\rho_l}{Dt}+\phi_l h_l\rho_l(\vec{\nabla}\cdot\vec{u})+\rho_l e_l\frac{D\phi_l}{Dt}\Big]+X=0. \tag{7.6}$$

Now, using Eqs. (3.5)–(3.6), one obtains

$$\sum_{l=1}^{2}\Big[\rho_l\phi_l T_l\frac{Ds_l}{Dt}+h_l\vec{\nabla}\cdot(\rho_l\vec{a}_l)-p_l(\vec{\nabla}\cdot\vec{a}_l)\Big]+X=0. \tag{7.7}$$

Hence, if $X=\sum_{l=1}^{2}\{p_l(\vec{\nabla}\cdot\vec{a}_l)-h_l\vec{\nabla}\cdot(\rho_l\vec{a}_l)\}$, then the condition in Eq. (7.1) is satisfied. Now, invoking the isobaric closure law (Section 3), $\sum_{l=1}^{2}\{p_l(\vec{\nabla}\cdot\vec{a}_l)\}=0$, and the proof is complete. □

The internal energy equation of the form in Eq. (7.2) does not satisfy the IEC, which also alludes to the fact that the entropy is not conserved exactly in a diffuse-interface method with regularization terms. Since we now only seek approximate entropy conservation, we modify the regularization term in Eq. (7.2) such that it satisfies the IEC, and the conservative form of the regularization term is restored. Thus, we arrive at the final form of the internal energy equation (taking the h_l on the right-hand side of Eq. (7.2) inside the divergence operator)

$$\frac{\partial\rho e}{\partial t}+\vec{\nabla}\cdot(\rho\vec{u}e)+\vec{\nabla}\cdot(p\vec{u})-\vec{u}\cdot\vec{\nabla}p=\sum_{l=1}^{2}\vec{\nabla}\cdot(\rho_l h_l\vec{a}_l). \tag{7.8}$$

In compressible flows, internal energy is not a conserved quantity, but the sum of internal and kinetic energy is conserved. Hence, summing up the internal energy transport equation (Eq. (7.8)) and the kinetic energy transport equation (Eq. (6.4)), we obtain

$$\frac{\partial E}{\partial t}+\vec{\nabla}\cdot(\vec{u}E)+\vec{\nabla}\cdot(p\vec{u})=\vec{\nabla}\cdot(\vec{f}\vec{k})+\sum_{l=1}^{2}\vec{\nabla}\cdot(\rho_l h_l\vec{a}_l). \tag{7.9}$$

Clearly, all the terms in this equation are in conservative form as desired, and since this equation was obtained by summing the forms of internal energy and kinetic energy equations that satisfied the IEC, this form of the total energy equation also satisfies the IEC. With the inclusion of viscous terms, we get the final form of the total energy transport equation in Eq. (3.8).

8. Interface equilibrium condition

In incompressible flows, the divergence-free condition constraints the velocity and pressure fields, and hence eliminates the possibility of any spurious solutions at the interface (in the absence of surface tension forces). However, such a constraint in compressible flows is absent, and thus care must be taken in the implementation of any numerical scheme in order to avoid spurious solutions at the interface. The IEC provides a consistency condition to check and eliminate the forms of the model and the numerical discretizations that contribute spuriously to the solution.

Lemma 8.1. *The proposed conservative diffuse-interface model in Eqs. (3.5)-(3.8) satisfies the IEC defined in Postulate (3.1).*

Proof.

Part (a). Mechanical equilibrium: uniform velocity across the interface

Consider a one-dimensional discretization of the mass balance equation (Eq. (3.6)) on a uniform grid, assuming $u_i^k = u_0$

$$(\rho_l\phi_l)_i^{k+1} - (\rho_l\phi_l)_i^k = -\Delta t\left[\frac{(\rho_l\phi_l)_{i+1} - (\rho_l\phi_l)_{i-1}}{2\Delta x}\right]^k u_0 + \Delta t\left[\frac{R_{l,i+1} - R_{l,i-1}}{2\Delta x}\right]^k, \quad (8.1)$$

where k is the timestep and i is the grid index. Now, consider a one-dimensional discretization of the momentum equation (Eq. (3.7)) on a uniform grid, assuming $u_i^k = u_0$ and $p_i^k = p_0$

$$(\rho u)_i^{k+1} - \rho_i^k u_0 = -\Delta t\left[\frac{\rho_{i+1} - \rho_{i-1}}{2\Delta x}\right]^k u_0^2 + \Delta t\left[\frac{\sum_{l=1}^2 R_{l,i+1} - \sum_{l=1}^2 R_{1,i-1}}{2\Delta x}\right]^k u_0. \quad (8.2)$$

Subtracting this from the sum of the discrete mass balance equations for phases 1 and 2 gives $u_i^{k+1} = u_0$.

Part (b). Thermodynamic equilibrium: Uniform pressure across the interface

Consider a one-dimensional discretization of the internal energy equation (Eq. (7.8)) on a uniform grid, assuming $u_i^k = u_0$ and $p_i^k = p_0$ and using Eq. (3.11)

$$\begin{aligned}\sum_{l=1}^2(\phi_l\rho_l e_l)_i^{k+1} - \sum_{l=1}^2(\phi_l\rho_l e_l)_i^k = -\Delta t\sum_{l=1}^2\left[\frac{(\rho_l e_l\phi_l)_{i+1} - (\rho_l e_l\phi_l)_{i-1}}{2\Delta x}\right]^k u_0 \\ +\Delta t\left[\sum_{l=1}^2\left\{\frac{p_0(1+\alpha_l) - \beta_l}{\alpha_l}\right\}\left\{\frac{a_{l,i+1} - a_{l,i-1}}{2\Delta x}\right\}\right]^k,\end{aligned} \quad (8.3)$$

and expressing e_l in terms of p_l using the EOS results in the discretized equation for pressure

$$\begin{aligned}&\Big(\sum_{l=1}^2\frac{\phi_l}{\alpha_l}\Big)^{k+1}p_i^{k+1} - \Big(\sum_{l=1}^2\frac{\phi_l\beta_l}{\alpha_l}\Big)^{k+1} - \Big(\sum_{l=1}^2\frac{\phi_l}{\alpha_l}\Big)^k p_0 + \Big(\sum_{l=1}^2\frac{\phi_l\beta_l}{\alpha_l}\Big)^k \\ &= -\Delta t\left[\frac{\Big(\sum_{l=1}^2\frac{\phi_l}{\alpha_l}\Big)_{i+1}p_0 - \Big(\sum_{l=1}^2\frac{\phi_l\beta_l}{\alpha_l}\Big)_{i+1} - \Big(\sum_{l=1}^2\frac{\phi_l}{\alpha_l}\Big)_{i-1}p_0 + \Big(\frac{\sum_{l=1}^2\phi_l\beta_l}{\alpha_l}\Big)_{i-1}}{2\Delta x}\right]^k u_0 \\ &\quad +\Delta t\left[\sum_{l=1}^2\left\{\frac{p_0(1+\alpha_l) - \beta_l}{\alpha_l}\right\}\left\{\frac{a_{l,i+1} - a_{l,i-1}}{2\Delta x}\right\}\right]^k.\end{aligned} \quad (8.4)$$

Now, let $L(\phi_l)$ be a one-dimensional discretization of the volume fraction advection equation for phase l (Eq. (3.5)) on a uniform grid. Assuming $u_i^k = u_0$, and subtracting Eq. (8.4) from the equation $\Big(\sum_{l=1}^2 L(\phi_l)/\alpha_l\Big)p_0 - \Big(\sum_{l=1}^2 L(\phi_l)\beta_l/\alpha_l\Big)$, results in $p_i^{k+1} = p_0$. □

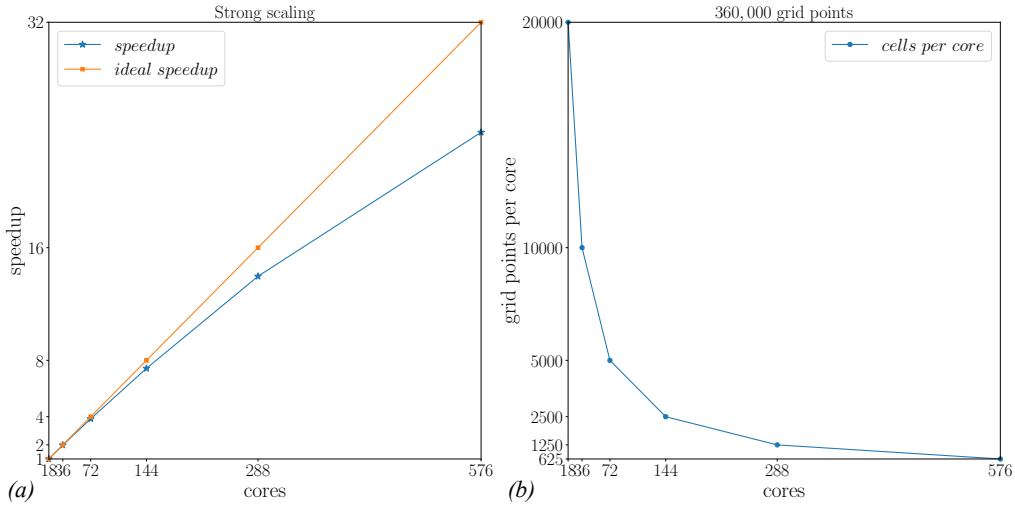

FIGURE 4. Strong scaling of the two-dimensional version of the solver on Mira, ANL. (a) Speedup is plotted against the number of cores for a test problem of size $360,000$ grid points. (b) The number of grid points per core is plotted against the number of cores for the same simulation.

9. Results

To verify the proposed model, we have written two versions of this solver in C++ (in two and three dimensions). This solver can also run in parallel using a Message Passing Interface (MPI) library with arbitrary Cartesian-based domain decomposition. The parallel-scaling efficiency of the two-dimensional version of this solver has been computed on the Mira supercomputer at Argonne National Laboratory (ANL), and the strong-scaling results are shown in Figure 4. For a test problem of size $360,000$ grid points, good strong scaling was achieved up to about 288 cores, i.e., up to 1250 grid points per core. Further rigorous scaling analyses on larger problems, the three-dimensional solver, and also the weak-scaling analyses will be presented in the future. The solver has been optimized by using contiguous memory allocations for the arrays and the amount of communication has been minimized by the use of custom-defined MPI datatypes.

In the rest of this section, two verification tests used to assess the newly proposed model are presented. The verification tests used in this work are (a) pressure-driven bubble oscillation and (b) the interaction of a plane acoustic wave with a flat air-water interface. In all the test cases, the fluids used are air and water, and their properties are listed in Table 1. In all the test cases, the initial profile of ϕ is analytically specified with an initial value of $\epsilon_0 = 2\Delta x$, unless specified otherwise.

9.1. *Rayleigh-Plesset equations*

For the test case of pressure-driven bubble oscillation, we compare the results against the analytical solution of the Rayleigh-Plesset equation. In three dimensions, the Rayleigh-Plesset equation can be written as (Brennen 2013)

$$\frac{P_B(t) - P_\infty(t)}{\rho} = R\ddot{R} + \frac{3}{2}(\dot{R})^2 + \frac{4\nu\dot{R}}{R} + \frac{2\sigma}{\rho R}, \tag{9.1}$$

	air	water
ρ (kg/m^3)	1.225	997
μ (N/m^2)	1.81e-5	8.9e-4
γ	1.4	4.4
π (MPa)	0	600

TABLE 1. Properties of the fluids used in this work.

where $P_B(t)$ is the uniform pressure inside the bubble, $P_\infty(t)$ is the liquid pressure at infinity, $R(t)$ is the radius of the bubble, ρ is the liquid density, ν is the liquid kinematic viscosity, σ is the surface tension, which is taken to be zero in this work, and each dot represents the $\mathrm{d}/\mathrm{d}t$. A two-dimensional Rayleigh-Plesset equation does not exist and cannot be derived due to the presence of a logarithmic singularity at infinity. However, a finite-domain analytical solution can still be derived and can be used to verify the numerical solution. Hence, we derive a two-dimensional equivalent of the Rayleigh-Plesset equation for finite-size domains. Typically, the Rayleigh-Plesset equation is derived by integrating the mass and momentum conservation equations in the liquid region around the bubble. The liquid is assumed to be incompressible, and the bubble is assumed to oscillate in only the first volumetric mode, which is axisymmetric in nature. Now, balancing the mass in the liquid region between the radius of the bubble, $R(t)$, and a distance r from the center of the bubble, we can write the radial velocity at a radius r as

$$u(r,t) = \frac{R(t)}{r}\frac{dR(t)}{dt}. \tag{9.2}$$

Starting with the radial component of the incompressible Navier-Stokes equation in polar coordinates

$$\frac{\partial u}{\partial t} + u\frac{\partial u}{\partial r} = -\frac{1}{\rho}\frac{\partial p}{\partial r} + \nu\left\{\frac{1}{r}\left[\frac{\partial}{\partial r}\left(r\frac{\partial u}{\partial r}\right)\right] - \frac{u}{r^2}\right\}, \tag{9.3}$$

and substituting for the velocity from Eq. (9.2), we obtain

$$\frac{1}{r}\left\{\left[\frac{\mathrm{d}R(t)}{\mathrm{d}t}\right]^2 + R(t)\frac{\mathrm{d}^2R(t)}{\mathrm{d}t^2}\right\} - \frac{R^2(t)}{r^3}\left[\frac{\mathrm{d}R(t)}{\mathrm{d}t}\right]^2 = -\frac{1}{\rho}\frac{\partial p}{\partial r}. \tag{9.4}$$

This equation is valid in the liquid region, and hence can be integrated from the surface of the bubble, $R(t)$. If we integrate this to infinity, we encounter a logarithmic singularity unlike in the three-dimensional Rayleigh-Plesset equation. To avoid this, we integrate Eq. (9.4) to a finite distance S from the center of the bubble and obtain

$$\frac{P_R(t) - P_S(t)}{\rho} = \ln\left\{\frac{S}{R(t)}\right\}\left\{\left[\frac{\mathrm{d}R(t)}{\mathrm{d}t}\right]^2 + R(t)\frac{\mathrm{d}^2R(t)}{\mathrm{d}t^2}\right\} + \left[\frac{R^2(t) - S^2}{2S^2}\right]\left(\frac{\mathrm{d}R(t)}{\mathrm{d}t}\right)^2, \tag{9.5}$$

where P_R and P_S are the liquid pressures at the surface of the bubble ($r = R$) and $r = S$, respectively. Now, balancing the pressure, viscous, and surface tension forces at the surface of the bubble

$$0 = -P_R(t) + 2\mu\frac{\partial u}{\partial r}[R(t),t] + P_B(t) - \frac{\sigma}{R(t)}, \tag{9.6}$$

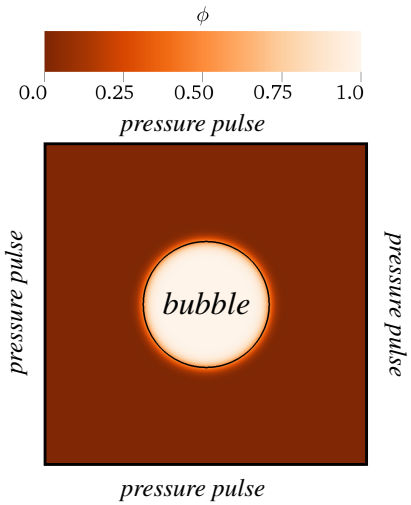

FIGURE 5. Schematic of the domain used in the case of pressure-driven bubble oscillation.

and substituting in Eq. (9.5), we obtain the two-dimensional equivalent of the Rayleigh-Plesset equation for the finite-size circular domain

$$\frac{P_B(t) - P_S(t)}{\rho} = \ln\left(\frac{S}{R}\right)\left\{(\dot{R})^2 + R\ddot{R}\right\} + \left(\frac{R^2 - S^2}{2S^2}\right)(\dot{R})^2 + \frac{2\nu\dot{R}}{R} + \frac{\sigma}{\rho R}. \tag{9.7}$$

9.2. *Pressure-driven bubble oscillation*

In this test case, an air bubble of diameter 4 μm is placed at the center of a square domain of size 10 μm × 10 μm, as shown in Figure 5. On all four sides of the domain, a Dirichlet boundary condition of the form $10^5\{1 + 0.1\sin(10\omega_c t)\}$ for the pressure and a Neumann boundary condition for the velocity are imposed, where $\omega_c = 10208967.75$ s^{-1} is the characteristic resonance frequency of the bubble (Minnaert 1933). The ϕ field is initialized with an analytical hyperbolic-tangent function (equilibrium solution of the volume fraction regularization term in Eq. (3.5)) given by $1 - 0.5\left\{1 + \tanh\left(\sqrt{x^2 + y^2} - r/\epsilon_0\right)\right\}$, where r is the radius of the bubble.

The solution was numerically integrated for a total of 50 μs physical time. Four different grid sizes were chosen, 50 × 50, 100 × 100, 200 × 200, and 600 × 600, to study the convergence of the solution. Timesteps were chosen based on the acoustic CFL condition for the particular grid size. The interface parameters $\Gamma = |u|_{max}$ and $\epsilon = \Delta x$ were used for all the simulations. Results from the various grid sizes are shown in Figure 6 and are compared with the semi-analytical solution obtained from numerically integrating the ordinary differential equation in Eq. (9.7) along with the ideal-gas law, where the bubble area is computed as $\int \phi dV$ in the simulations. Figure 6 shows the bubble response at initial times (0 μs to 0.6 μs) and at later times (20 μs to 20.25 μs). The initial transient response of the bubble shows a clear convergence of the numerical solution to the analytical solution with the increase in grid size. Moreover, the solution is very accurate even on the coarsest grid for the bubble response at later times (Figure 6(b)). This test case also shows that the numerical solution is stable for long-time integrations.

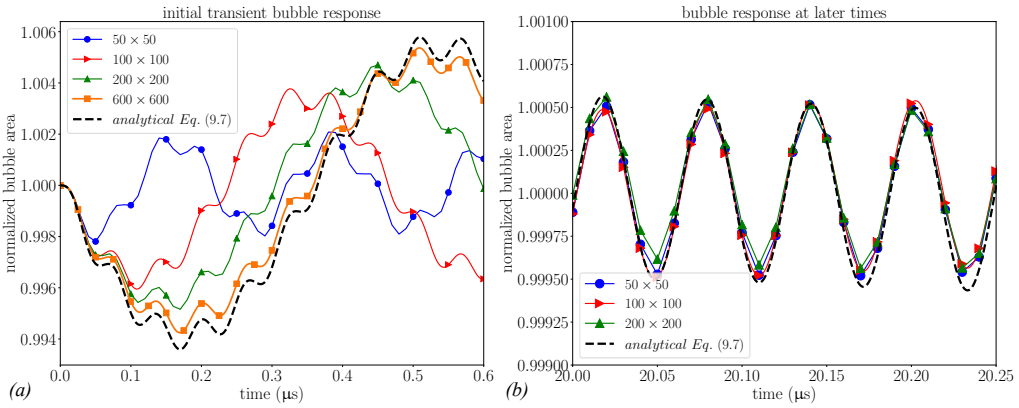

FIGURE 6. Bubble response at (a) initial and (b) later times.

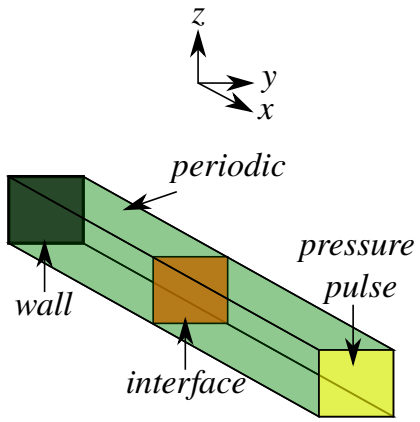

FIGURE 7. Schematic of the domain used in the case of interaction of a plane acoustic wave with a flat air-water interface.

9.3. *Interaction of a plane acoustic wave with a flat air-water interface*

In this test case, a long three-dimensional domain of size 10 μm × 0.1 μm × 0.1 μm is used, with a flat air-water interface located at $x = 5$ μm, as shown in Figure 7. The domain is filled with air for $x < 5$ μm and water for $x > 5$ μm. Perflectly reflecting wall boundary conditions are imposed on the domain face at $x = 0$ μm, and periodic boundary conditions are imposed for the faces at $y = 0$ μm, $y = 0.1$ μm, $z = 0$ μm, and $z = 0.1$ μm. For the wall at $x = 10$ μm, a Dirichlet boundary condition of the form $10^5\{1 - 0.5\sin(c2\pi/\lambda t)\}$ for the pressure and a Neumann boundary condition for the velocity are imposed for $t < 614.5$ ps, where $\lambda = 1$ μm and c is the speed of sound in water. Later, it is switched to a perfectly reflecting wall boundary conditions for $t > 614.5$ ps such that a half-wave is generated at the boundary and its propagation in the domain can be monitored. The ϕ field is initialized with the analytical function $1 - 0.5\Big\{1 + \tanh\Big(x - x_0/\epsilon_0\Big)\Big\}$, where x_0 is the location of the interface.

The solution was numerically integrated for a total of 1 μs physical time. A grid of size $1000 \times 10 \times 10$ was used in this simulation along with the timestep size of $\Delta t = 1$ps. The

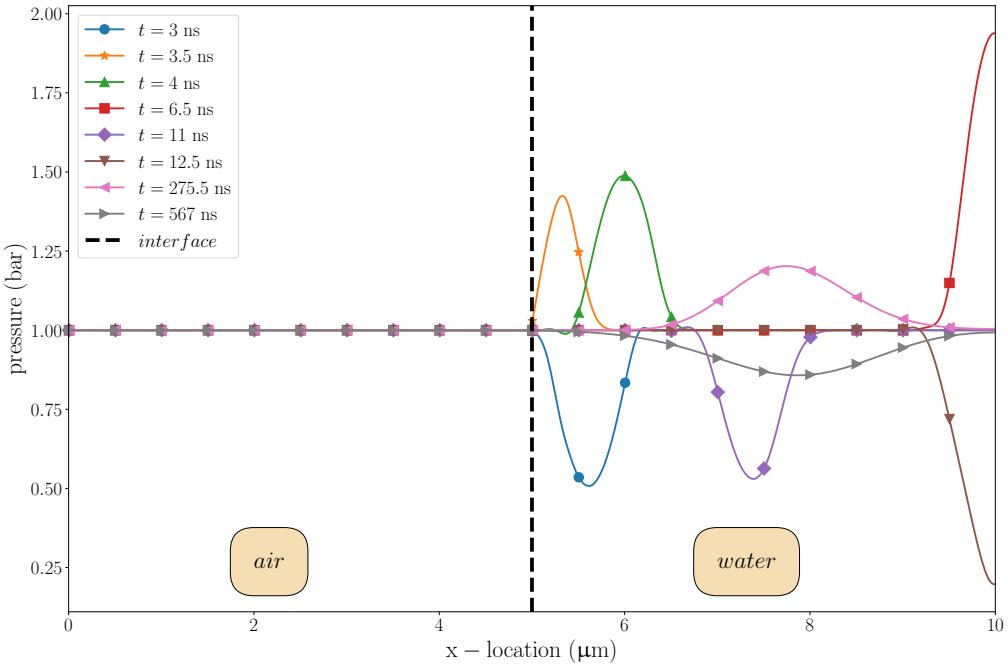

FIGURE 8. Line plot of pressure along x at various times.

interface parameters $\Gamma = |u|_{max}$ and $\epsilon = \Delta x$ were used for all the simulations. Results from the simulation are shown in Figure 8. The pressure along x is plotted at various times for $y = z = 0.05$ μm. The acoustic wave interacts with the air-water interface and reflects back, as can be seen from the results at 3ns, 3.5ns and 4ns. Clearly, nothing gets transmitted across the interface, and the reflected wave amplitude is approximately equal to the incident wave amplitude but the wave is flipped. This behavior of reflection and transmission of an acoustic wave across a flat air-water interface can be predicted using linear acoustic theory. The reflection coefficient is given by $\mathbb{R} = (Z_a - Z_w)/(Z_a + Z_w) = -0.999516$, and the transmission coefficent is given by $\mathbb{T} = 2Z_a/(Z_a + Z_w) = 4.8 \times 10^{-3}$, where Z_a and Z_w are the acoustic impedance for air and water, respectively. $\mathbb{R}$ being roughly equal to -1 indicates that the reflected wave amplitude is the same as the incident wave amplitude and the wave is flipped. $\mathbb{T}$ being roughly equal to 0 indicates that nothing gets transmitted across the interface. Hence, the numerical solution is in good agreement with the theoretical prediction. Solutions at 6.5ns and 12.5ns also show the pressure-doubling behavior at the wall, which is again predicted by the theory (Blackstock 2000).

10. Summary and future work

In this study, we propose a conservative diffuse-interface method for the simulation of compressible two-phase flows with turbulence and acoustics. The advantages of our method compared to the state-of-the-art methods are (a) discrete mass, momentum, and total energy conservation, (b) non-dissipative spatial discretization, (c) stability for long-time integrations, (d) thermodynamic consistency at the interface, and (e) kinetic

energy conservation (i.e., no spurious contribution to the solution) and approximate entropy conservation.

Current study is focused on a shock-free compressible regime (low-Mach number regime), but shocks in a high-Mach number regime can potentially be handled with the implementation of the localized artificial bulk viscosity approach (Mani *et al.* 2009; Kawai *et al.* 2010). Furthermore, extensions to include surface tension, dispersion-relation preserving schemes, and skew-symmetic splitting (Honein 2005) are being tested and will also be discussed in future work.

Acknowledgments

This investigation was funded by the Office of Naval Research, Grants #N00014-15-1-2726 and #N00014-15-1-2523, and the Advanced Simulation and Computing (ASC) program of the US Department of Energy's National Nuclear Security Administration via the PSAAP-II Center at Stanford, Grant No. DE-NA0002373. S. S. Jain is also funded by a Franklin P. and Caroline M. Johnson Fellowship. The authors acknowledge computational resources from the US DoE's INCITE Program, as well as from the Certainty cluster awarded by the National Science Foundation to CTR. The authors are grateful to Shahab Mirjalili for fruitful discussions, and to Javier Urzay for motivating this study.

REFERENCES

Abgrall, R. 1996 How to prevent pressure oscillations in multicomponent flow calculations: a quasi conservative approach. *J. Comput. Phys.* **125**, 150–160.

Allaire, G., Clerc, S. & Kokh, S. 2002 A five-equation model for the simulation of interfaces between compressible fluids. *J. Comput. Phys.* **181**, 577–616.

Baer, M. & Nunziato, J. 1986 A two-phase mixture theory for the deflagration-to-detonation transition (DDT) in reactive granular materials. *Int. J. Multiph. Flow* **12**, 861–889.

Blackstock, D. T. 2000 *Fundamentals of Physical Acoustics*. John Wiley & Sons.

Brennen, C. E. 2013 *Cavitation and Bubble Dynamics*. Cambridge University Press.

Carrica, P., Drew, D., Bonetto, F. & Lahey Jr, R. 1999 A polydisperse model for bubbly two-phase flow around a surface ship. *Int. J. Multiph. Flow* **25**, 257–305.

Culver, R. L. & Trujillo, M. F. 2007 Measuring and modeling bubbles in ship wakes, and their effect on acoustic propagation. In *Proc. 2nd Int. Conf. Underwater Acoustic Measurements*.

Fu, L., Hu, X. Y. & Adams, N. A. 2017 Single-step reinitialization and extending algorithms for level-set based multi-phase flow simulations. *Comput. Phys. Commun.* **221**, 63–80.

Fu, T., Karion, A., Fullerton, A., Rice, J. & Walker, D. 2007 Characterization of the bubble flow and transom wave of the R/V Athena I. *Tech. Rep.* NSWCCD-50-TR-2007/049. Naval Surface Warfare Center.

He, Z., Tian, B., Zhang, Y. & Gao, F. 2017 Characteristic-based and interface-sharpening algorithm for high-order simulations of immiscible compressible multi-material flows. *J. Comput. Phys.* **333**, 247–268.

Herrmann, M. 2016 A sharp interface in-cell-reconstruction method for volume tracking phase interfaces in compressible flows. *Proceedings of the Summer Program*, Center for Turbulence Research, Stanford University, pp. 5–14.

Honein, A. E. 2005 Numerical aspects of compressible turbulence simulations. PhD thesis, Stanford University.

Huber, G., Tanguy, S., Béra, J.-C. & Gilles, B. 2015 A time splitting projection scheme for compressible two-phase flows. application to the interaction of bubbles with ultrasound waves. *J. Comput. Phys.* **302**, 439–468.

Jemison, M., Sussman, M. & Arienti, M. 2014 Compressible, multiphase semi-implicit method with moment of fluid interface representation. *J. Comput. Phys.* **279**, 182–217.

Kapila, A., Menikoff, R., Bdzil, J., Son, S. & Stewart, D. S. 2001 Two-phase modeling of deflagration-to-detonation transition in granular materials: Reduced equations. *Phys. Fluids* **13**, 3002–3024.

Kawai, S., Shankar, S. K. & Lele, S. K. 2010 Assessment of localized artificial diffusivity scheme for large-eddy simulation of compressible turbulent flows. *J. Comput. Phys.* **229**, 1739–1762.

Mani, A., Larsson, J. & Moin, P. 2009 Suitability of artificial bulk viscosity for large-eddy simulation of turbulent flows with shocks. *J. Comput. Phys.* **228**, 7368–7374.

Minnaert, M. 1933 XVI. On musical air-bubbles and the sounds of running water. *Lond.Edinb.Dubl.Phil.Mag.J.Sci.* **16**, 235–248.

Mirjalili, S., Ivey, C. B. & Mani, A. 2018 A conservative diffuse interface method for two-phase flows with provable boundedness properties. *arXiv:1803.01262v2*.

Mirjalili, S. & Mani, A. 2019 *Manuscript in preparation*.

Mirjalili, S., Jain, S. S. & Dodd, M. 2017 Interface-capturing methods for two-phase flows: An overview and recent developments. *Annual Research Briefs*, Center for Turbulence Research, Stanford University, pp. 117–135.

Moin, P. & Verzicco, R. 2016 On the suitability of second-order accurate discretizations for turbulent flow simulations. *Eur. J. Mech. B Fluids* **55**, 242–245.

Olsson, E. & Kreiss, G. 2005 A conservative level set method for two phase flow. *J. Comput. Phys.* **210**, 225–246.

Olsson, E., Kreiss, G. & Zahedi, S. 2007 A conservative level set method for two phase flow II. *J. Comput. Phys.* **225**, 785–807.

Saurel, R. & Pantano, C. 2018 Diffuse-interface capturing methods for compressible two-phase flows. *Annu. Rev. Fluid Mech.* **50**, 105–130.

Shukla, R. K., Pantano, C. & Freund, J. B. 2010 An interface capturing method for the simulation of multi-phase compressible flows. *J. Comput. Phys.* **229**, 7411–7439.

Stanic, S., Caruthers, J. W., Goodman, R. R., Kennedy, E. & Brown, R. A. 2009 Attenuation measurements across surface-ship wakes and computed bubble distributions and void fractions. *IEEE J. Ocean. Eng.* **34**, 83–92.

Tiwari, A., Freund, J. B. & Pantano, C. 2013 A diffuse interface model with immiscibility preservation. *J. Comput. Phys.* **252**, 290–309.

Trevorrow, M. V., Vagle, S. & Farmer, D. M. 1994 Acoustical measurements of microbubbles within ship wakes. *J. Acoust. Soc. Am.* **95**, 1922–1930.

Versteeg, H. K. & Malalasekera, W. 2007 *An Introduction to Computational Fluid Dynamics: The Finite Volume Method*. Pearson Education.